Check for updates

Effect of scission on alignment of nonionic surfactant micelles under shear flow

Yusuke Koide ⓘD * and Susumu Goto ⓘD

We investigate the alignment of wormlike micelles under shear flow with dissipative particle dynamics simulations of nonionic surfactant solutions. To reveal the effect of micellar scission on alignment, we evaluate the shear-rate dependence of the mean orientation angle and the average lifetime of micelles for fixed aggregation numbers. Our numerical results demonstrate the presence of two distinct shear-rate regimes of micellar alignment. In the low shear-rate regime, where flow-induced scission does not occur, wormlike micelles align more in the flow direction with the shear rate. In contrast, flow-induced scission suppresses micellar alignment in the high shear-rate regime. In addition, comparing the alignment of wormlike micelles with that of polymers without scission, we find that the mean orientation angle of wormlike micelles is larger than that of polymers when flow-induced scission occurs. This comparison confirms that flow-induced scission yields the unique behavior of micellar alignment. Furthermore, we demonstrate that flow-induced scission suppresses micellar alignment for fixed aggregation numbers by reducing the effective longest relaxation time of micelles.

1. Introduction

One of the significant differences between polymers and wormlike micelles is the underlying mechanism of their structure formation. Polymers are based on covalent bonds, whereas surfactant micelles are on weak non-bonded interactions. Thus, unlike polymers, micelles constantly exhibit scission and recombination. It is important to understand how this difference affects their properties. A crucial example is turbulent drag reduction by adding polymers and surfactants.[1,2] Since the flow statistics are similar for both additives,[3] polymers and surfactant micelles have similar roles in modulating turbulence. However, there is an indispensable difference originating from their formation mechanisms. Since polymers are formed through covalent bonds, their structures never recover once they are broken by strong shear flows.[4] Due to this irreversibility, the drag reduction efficiency by polymer additives declines with time.[5–7] In contrast, since the driving force for micellization is a non-bonded interaction, surfactants can form micelles again after scission.[8] Thus surfactant solutions are less affected by mechanical degradation than polymers.[9] This property makes surfactants more suitable for closed-loop systems such as air conditioning systems.[10,11] Therefore, developing technologies using polymer and surfactant solutions requires a fundamental knowledge of their different properties arising from their formation mechanisms.

Here, we explore whether micellar scission kinetics yields a difference in alignment behavior under shear flow. In general, the alignment of wormlike micelles and polymers is closely related to the rheological properties of their solutions. Since surfactants and polymers are often added to solutions to control rheology,[12–14] it is indispensable to understand their alignment properties. Many studies have been conducted on polymer alignment using theoretical, experimental, and numerical approaches.[15–18] It is well known that polymers under shear flow align more in the flow direction as the shear rate increases. Similarly to polymers, numerous studies have reported that rodlike and wormlike micelles also align in the flow direction.[19–26] However, little is known about the effect of scission on micellar alignment, although recent experimental results suggest that the scission effect on the micellar alignment emerges for high shear rates. Arenas-Gómez *et al.*[25] conducted simultaneous measurements of the viscosity and alignment of wormlike micelle solutions. They revealed that the orientation parameter exhibits nonmonotonic dependence on the shear rate. They attributed the decrease in the orientation parameter to the decreased contour length due to increased scission frequency. Recently, King *et al.*[26] investigated the alignment and viscosity of concentrated wormlike micelle solutions. They demonstrated that the saturation of alignment occurs for high shear rates, indicating the scission effect. However, it is difficult to experimentally measure the scission frequency and observe the structures and dynamics of individual micelles in flowing solutions. Thus the effect of scission on micellar alignment remains unclear.

Graduate School of Engineering Science, Osaka University, 1-3 Machikaneyama, Toyonaka, Osaka 560-8531, Japan. E-mail: y_koide@fm.me.es.osaka-u.ac.jp

Molecular simulations allow us to overcome these difficulties and reveal the relationship between alignment and scission. Although some studies investigated the alignment of rodlike and wormlike micelles using molecular simulations,[27–30] little has been done to reveal the effect of scission.[31] Huang *et al.*[28] used a mesoscopic model incorporating a kinetic model for scission and recombination into linear chains and examined alignment and scission under shear flow. Although they reported the saturation of alignment for high shear rates, they attributed this saturation to finite-size effects under strong shear flows. Sambasivam *et al.*[30] investigated alignment and scission of a single rodlike micelle under shear flow with the coarse-grained molecular dynamics (CGMD) method. They found that when the Weissenberg number Wi = $\tau\dot{\gamma}$ defined as the product of the shear rate $\dot{\gamma}$ and the rotational relaxation time τ is larger than 1, a rodlike micelle aligns in the flow direction exhibiting tumbling dynamics. They also showed that elongation of micelles by shear flow leads to micellar scission for large Wi. However, there was no comparison between alignment and scission for given Wi. Although it is worth noting that Carl *et al.*[31] found that the saturation of the mean alignment angle can occur due to a decrease in the average chain length, there is still room for studying micellar alignment under shear flow in terms of scission.

In the present study, we investigate the effect of scission on micellar alignment through detailed analysis of both alignment and scission using molecular simulations. There are two significant issues for solving this problem. One is the evaluation of statistical properties of scission. Observing many scission events requires a high computational cost. To overcome this difficulty, we employ the dissipative particle dynamics (DPD) method. Thanks to coarse-graining and soft repulsive interactions, DPD allows us to simulate large systems for long time scales with a low computational cost. In fact, our previous study[32] demonstrated that DPD is suitable for evaluating the statistical properties of micellar lifetimes. In addition, surfactant and water molecules are explicitly considered in DPD simulations. Thus we do not rely on a kinetic model for the scission and recombination of micelles.[33–35] The other issue is the polydispersity of the aggregation number of micelles. When a concentration is high enough for wormlike micelles to exist, micelles of different sizes coexist in the solution. In addition, the distribution changes for high shear rates due to increased scission frequency.[32] Thus statistics over all the micelles in the system, often used in previous studies,[28,29,33,36] could demonstrate only the combined effect of the changes in the micellar properties and distributions. Here, we employ conditional statistics based on the aggregation number used in our previous study.[32] This analysis method separates the effect of individual micellar properties and distributions of the aggregation number. In addition, this method allows us to directly compare the alignment of individual micelles with that of polymers to reveal the effect of micellar scission on alignment. In the following, we will quantitatively show that flow-induced scission suppresses micellar alignment even for fixed aggregation numbers.

2. Method

2.1 DPD governing equations

In the present study, we use the DPD method to conduct molecular simulations of nonionic surfactant solutions. In DPD simulations, a single DPD particle represents a group of atoms and molecules. The motion of a DPD particle obeys

$$m_i\frac{\mathrm{d}\boldsymbol{v}_i}{\mathrm{d}t} = \sum_{j(\neq i)}\boldsymbol{F}_{ij}^{\mathrm{C}} + \sum_{j(\neq i)}\boldsymbol{F}_{ij}^{\mathrm{D}} + \sum_{j(\neq i)}\boldsymbol{F}_{ij}^{\mathrm{R}}, \quad (1)$$

where m_i and $\boldsymbol{v}_i$ are the mass and velocity of the ith particle, respectively; and $\boldsymbol{F}_{ij}^{\mathrm{C}}$, $\boldsymbol{F}_{ij}^{\mathrm{D}}$, and $\boldsymbol{F}_{ij}^{\mathrm{R}}$ are the conservative, dissipative, and random forces exerted on the ith particle by the jth particle, respectively. Note that the bond force $\boldsymbol{F}_{ij}^{\mathrm{B}}$ is added in eqn (1) for surfactants and polymers. The conservative force acts as a repulsive force in the form of

$$\boldsymbol{F}_{ij}^{\mathrm{C}} = \begin{cases} a_{ij}\left(1 - \dfrac{r_{ij}}{r_{\mathrm{c}}}\right)\boldsymbol{e}_{ij} & \text{for } r_{ij} \leq r_{\mathrm{c}} \\ 0 & \text{for } r_{ij} > r_{\mathrm{c}}, \end{cases} \quad (2)$$

where a_{ij} is the conservative force coefficient between the ith and jth particles, r_{c} is the cutoff distance, $\boldsymbol{r}_{ij} = \boldsymbol{r}_i - \boldsymbol{r}_j$, $r_{ij} = |\boldsymbol{r}_{ij}|$, and $\boldsymbol{e}_{ij} = \boldsymbol{r}_{ij}/r_{ij}$ with $\boldsymbol{r}_i$ being the position of the ith particle. The dissipative and random forces are expressed as

$$\boldsymbol{F}_{ij}^{\mathrm{D}} = -\gamma w^{\mathrm{D}}(r_{ij})(\boldsymbol{e}_{ij}\cdot\boldsymbol{v}_{ij})\boldsymbol{e}_{ij} \quad (\boldsymbol{v}_{ij} = \boldsymbol{v}_i - \boldsymbol{v}_j) \quad (3)$$

and

$$\boldsymbol{F}_{ij}^{\mathrm{R}} = \sigma w^{\mathrm{R}}(r_{ij})\theta_{ij}\boldsymbol{e}_{ij}, \quad (4)$$

where γ and σ are the dissipative and random force coefficients, respectively; and $w^{\mathrm{D}}(r_{ij})$ and $w^{\mathrm{R}}(r_{ij})$ are the weight functions of the dissipative and random forces, respectively. In eqn (4), θ_{ij} is a random variable that satisfies

$$\theta_{ij}(t) = \theta_{ji}(t) \quad (5)$$

$$\langle\theta_{ij}(t)\rangle = 0 \quad (6)$$

$$\langle\theta_{ij}(t)\theta_{kl}(t')\rangle = (\delta_{ik}\delta_{jl} + \delta_{il}\delta_{jk})\delta(t - t') \quad (7)$$

where δ_{ij} is the Kronecker delta, $\delta(t)$ is the delta function, and $\langle\cdot\rangle$ denotes the ensemble average. The fluctuation dissipation theorem requires that γ, σ, $w^{\mathrm{D}}(r_{ij})$, and $w^{\mathrm{R}}(r_{ij})$ satisfy

$$w^{\mathrm{D}}(r_{ij}) = [w^{\mathrm{R}}(r_{ij})]^2 \quad (8)$$

and

$$\sigma^2 = 2\gamma k_{\mathrm{B}}T, \quad (9)$$

where k_{B} is the Boltzmann constant and T is the temperature of the system.[37] Following ref. 38, we set the weight function $w^{\mathrm{R}}(r_{ij})$ as

$$w^{\mathrm{R}}(r_{ij}) = \begin{cases} 1 - \dfrac{r_{ij}}{r_{\mathrm{c}}} & \text{for } r_{ij} \leq r_{\mathrm{c}} \\ 0 & \text{for } r_{ij} > r_{\mathrm{c}}. \end{cases} \quad (10)$$

In what follows, we use simulation units with $k_{\mathrm{B}}T = m = r_{\mathrm{c}} = 1$.

2.2 Surfactant model

The model of a nonionic surfactant molecule contains a hydrophilic head particle and two hydrophobic tail particles.

Table 1 DPD simulation parameters for surfactant solutions. N is the total number of DPD particles, ρ is the number density of DPD particles, σ is the random force coefficient, ϕ is the volume fraction of surfactants, k_s is the spring constant, r_{eq} is the equilibrium bond distance, and a_{ij} is the conservative force coefficient between different types of particles. The subscripts indicate the types of particles; namely, h, t, and w denote head, tail, and water particles, respectively

N	ρ	σ	ϕ	k_s	r_{eq}	a_{hh}	a_{ht}	a_{hw}	a_{tt}	a_{tw}	a_{ww}
648 000	3	3	0.05	50	0.8	25	60	20	25	60	25

Three surfactant particles are connected by two harmonic springs expressed by

$$\boldsymbol{F}_{ij}^{B} = -k_s(r_{ij} - r_{eq})\boldsymbol{e}_{ij}, \tag{11}$$

where k_s is the spring constant and r_{eq} is the equilibrium bond distance. Table 1 shows the simulation parameters for surfactant solutions. Here, N is the total number of DPD particles, ρ is the number density of DPD particles, ϕ is the volume fraction of surfactants, and a_{ij} is the conservative force coefficient between different types of particles. The subscripts indicate the types of particles; namely, h, t, and w denote head, tail, and water particles, respectively. We choose $\phi = 0.05$ because a sufficient number of wormlike micelles exist in the system with this volume fraction, as confirmed in our previous study.[32] Additionally, there is no entanglement effect in the considered system because the mean squared displacement of surfactants (see Fig. 6 of ref. 32) does not exhibit a power law specific to a reptation motion.[39] DPD simulations of surfactant solutions are performed in a cubic box of size $60 \times 60 \times 60$.

2.3 Polymer model

In the present study, we conduct DPD simulations of polymer solutions for comparison. We employ the fully flexible polymer model used in the previous study.[40] Linear polymer chains consist of N_m beads, and adjacent beads in a polymer are connected by finitely extensible nonlinear elastic (FENE) springs expressed by

$$\boldsymbol{F}_{ij}^{B} = -\frac{k_F(r_{ij} - r_{eq})\boldsymbol{e}_{ij}}{1 - \{(r_{ij} - r_{eq})/(r_{max} - r_{eq})\}^2}, \tag{12}$$

where k_F is the spring constant and r_{max} is the maximum bond distance. Table 2 shows the simulation parameters for polymer

Table 2 DPD simulation parameters for polymer solutions. N is the total number of DPD particles, N_m is the number of beads in a chain, ρ is the number density of DPD particles, σ is the random force coefficient, ϕ is the volume fraction of polymers, k_F is the spring constant, r_{eq} is the equilibrium bond distance, r_{max} is the maximum bond distance, and a_{ij} is the conservative force coefficient between different types of particles. The subscripts indicate the types of particles; namely, p and w denote polymer and water particles, respectively

N	N_m	ρ	σ	ϕ	k_F	r_{eq}	r_{max}	a_{pp}	a_{pw}	a_{ww}
375 000	50	3	3	0.05	40	0.7	2	25	25	25

solutions. DPD simulations of polymer solutions are performed in a cubic box of size $50 \times 50 \times 50$.

2.4 Simulation details

To integrate the equations of motion, we use the modified velocity Verlet method[38] with the time step $\Delta t = 0.04$ and the parameter $\lambda = 0.65$ introduced in this algorithm. We have confirmed that these parameters realize sufficiently accurate temperature control. To generate a uniform shear flow, we use the Lees–Edwards boundary condition[41] and the SLLOD equations.[42] We impose a random initial configuration and conduct equilibrium simulations for 20 000 time units for surfactant solutions and 8000 time units for polymer solutions, achieving statistically steady values of the potential energy. After that, we conduct non-equilibrium simulations by imposing shear flow. Conditional statistics for micelles introduced in Section 2.5 require DPD simulations for a long time to obtain sufficiently accurate results. Thus we conduct non-equilibrium simulations of surfactant solutions for 40 000–160 000 time units depending on the shear rate.

We perform all the DPD simulations using our in-house code.

2.5 Analysis details

To evaluate individual micellar properties, we need to identify micelles in the system. We define micelles adopting the method used in previous studies.[43,44] In this method, two surfactant molecules belong to a common cluster if a hydrophobic particle of one surfactant molecule is within r_c (=1) of a hydrophobic particle of the other. If a cluster has an aggregation number N_{ag} larger than a threshold value n_{mic} (=10), then we regard the cluster as a micelle. Since we focus mainly on micelles with $N_{ag} \gtrsim 50$, our results are practically insensitive to the choice of n_{mic}.

To investigate N_{ag} dependence of micellar properties, we use conditional statistics based on N_{ag} instead of statistics over all the micelles in the system. Specifically, to evaluate the micellar properties for given N_{ag}, we use the data for micelles having aggregation numbers that lie in $[N_{ag} - \Delta N_{ag}, N_{ag} + \Delta N_{ag}]$, where we set $\Delta N_{ag} = 0.05 N_{ag}$. In the following, the micellar orientation angle is conditioned by instantaneous N_{ag}, whereas the micellar lifetime is conditioned by the value of N_{ag} before scission.

3. Results

One of the most intriguing observations in the present study is that flow-induced scission, which occurs for high shear rates, suppresses micellar alignment in the flow direction even for fixed aggregation numbers N_{ag}. To quantitatively demonstrate the effect of scission on micellar alignment, we evaluate the shear-rate dependence of the micellar lifetime and alignment.

3.1 Alignment

In this subsection, we examine the micellar alignment under shear flow. First, we define micellar orientation angles. In the present study, we define the micellar direction as the
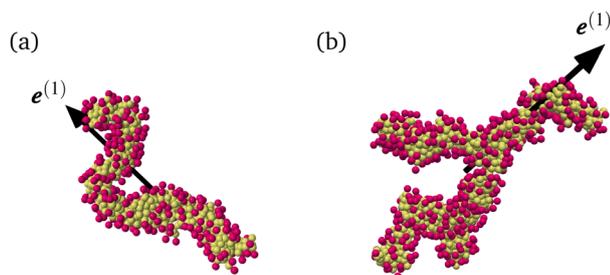
Fig. 1 Eigenvector $e^{(1)}$ of the gyration tensor G_{ij} corresponding to the largest eigenvalue for (a) N_{ag} = 300 and (b) N_{ag} = 500. Hydrophilic and hydrophobic particles are indicated in red and yellow, respectively.

eigenvector $e^{(1)}$ of the gyration tensor G_{ij} corresponding to the largest eigenvalue. Here, G_{ij} is defined as

$$G_{ij} = \frac{1}{N_{sur}} \sum_{k=1}^{N_{sur}} \Delta r_{k,i} \Delta r_{k,j}, \qquad (13)$$

where $\Delta r_{k,i}$ is the ith component of the relative position vector of the kth surfactant particle with respect to the center of mass of the micelle, and N_{sur} (=$3N_{ag}$) is the number of surfactant particles in the micelle. Fig. 1 shows the micellar structures and the corresponding $e^{(1)}$. We confirm that $e^{(1)}$ represents the global orientation of micelles. Since micelles form branched structures more often as N_{ag} increases (see Fig. 12 of ref. 32), it may also be important to consider the local orientation of branched micelles as shown in Fig. 1(b). However, for simplicity, we investigate the global alignment using $e^{(1)}$ in the following. Fig. 2 shows the definition of micellar angles θ and φ. To investigate micellar alignment in the flow direction, we focus on φ. Note that $\varphi \in [-\pi/2, \pi/2]$ because $e^{(1)}$ is equivalent to $-e^{(1)}$ in our definition.

A key point of our analysis is that we rely on conditional statistics based on N_{ag} instead of statistics over all the micelles in the system. The inset of Fig. 3 shows the probability density function (PDF) $P(N_{ag})$ of N_{ag} for the shear rate $\dot{\gamma}$ = 0.005. Note that the temporally averaged values are shown. We find that micelles of various sizes coexist in the system for the considered volume fraction ϕ. Fig. 3 shows the PDF $P(\varphi)$ of φ for various N_{ag}, which demonstrates that the statistical properties
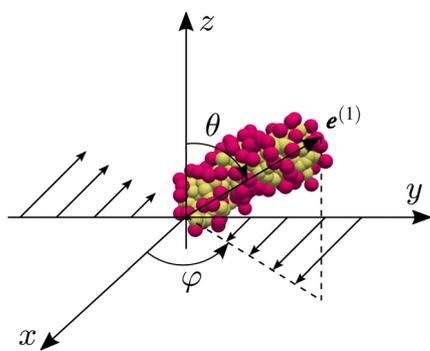

Fig. 2 Definition of angles θ and φ of micelles. The micellar direction is defined as the eigenvector $e^{(1)}$ of the gyration tensor G_{ij} corresponding to the largest eigenvalue.
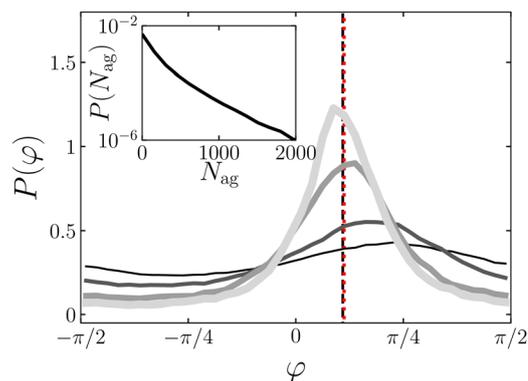

Fig. 3 PDF $P(\varphi)$ of the orientation angle φ for $\dot{\gamma}$ = 0.005. Different curves correspond to different values of the aggregation number: N_{ag} = 70, 100, 200, and 400 from thinner (and darker) to thicker (and lighter) lines. The inset shows PDF $P(N_{ag})$ of N_{ag} for $\dot{\gamma}$ = 0.005. The vertical black dashed line indicates the mean orientation angle $\bar{\varphi}$ defined by eqn (14), and the vertical dotted red line indicates the conventional mean orientation angle χ_G defined by eqn (15) for N_{ag} = 400.

of micellar alignment significantly depend on N_{ag} for given $\dot{\gamma}$. Therefore, the analysis using the information on all the micelles in the system, as conducted in previous studies,[28,29] reflects not only individual micellar dynamics but also the distribution of N_{ag}. In particular, since $P(N_{ag})$ for high shear rates greatly differ from that at equilibrium due to flow-induced scission (see Fig. 10 of ref. 32), this change in $P(N_{ag})$ complicates the interpretation of the results. We overcome this difficulty using conditional statistics based on N_{ag} defined in Section 2.5, which enables us to investigate the alignment properties of individual micelles.

In the following, we characterize $\dot{\gamma}$ dependence of micellar alignment with a mean orientation angle. Note that given a set of n angles $\{\varphi_1, \varphi_2, \ldots, \varphi_n\}$, the arithmetic mean $\sum_{i=1}^{n} \varphi_i/n$ is inappropriate as a mean orientation angle due to the periodicity of φ_i. For instance, the arithmetic mean of $\varphi_1 = \pi/2 - \varepsilon$ and $\varphi_2 = -\pi/2 + \varepsilon$ is zero even when $\varepsilon \ll 1$, which is misleading because $\varphi_1 \simeq \varphi_2 \simeq \pi/2$ modulo π. Here, we define a mean orientation angle $\bar{\varphi}$ as

$$\overline{\varphi} = \frac{1}{2} \arg\left(\frac{1}{n} \sum_{i=1}^{n} e^{2i\varphi_i} \right), \qquad (14)$$

where arg $(\cdot)$ denotes the argument of a complex number.[45] Doubling φ_i leads to $2\varphi_i \in [-\pi, \pi)$. Instead of the arithmetic mean of $2\varphi_i$, we consider that of $e^{2i\varphi_i}$ to avoid the problem due to the periodicity. Then we obtain $\bar{\varphi}$ by dividing the mean direction $\arg\left(\sum_{i=1}^{n} e^{2i\varphi_i}/n \right)$ of $2\varphi_i$ by 2. We show $\bar{\varphi}$ of micelles with N_{ag} = 400 for $\dot{\gamma}$ = 0.005 by a vertical black dashed line in Fig. 3 as an example. It verifies that $\bar{\varphi}$ is a characteristic angle of wormlike micelles. For comparison, we also show the conventional mean orientation angle χ_G[17,46] defined by

$$\tan(2\chi_G) = \frac{2G_{xy}}{G_{xx} - G_{yy}} \qquad (15)$$

in Fig. 3. We observe that $\bar{\varphi}$ and χ_G show similar values. Thus the definition of the mean orientation angle has little effect on the following results.

Fig. 4 shows $\dot{\gamma}$ dependence of $\bar{\varphi}$ for various N_{ag}. Two important features are evident in this result. First, N_{ag} dependence of $\bar{\varphi}$ for fixed $\dot{\gamma}$ indicates that there exists a threshold aggregation number N_Λ above which $\bar{\varphi}$ remains constant. For $N_{ag} \geq 300$, $\bar{\varphi}$ collapses on a single function of $\dot{\gamma}$ irrespective of N_{ag}. In contrast, $\bar{\varphi}$ of micelles with $N_{ag} \leq 130$ decreases as N_{ag} increases for fixed $\dot{\gamma}$. These observations indicate that the longest relaxation time of micelles increases with N_{ag} for $N_{ag} \lesssim N_\Lambda$ and remains constant for $N_{ag} \gtrsim N_\Lambda$. We will explain how to evaluate the values of the longest relaxation time and N_Λ in Section 4. Second, $\dot{\gamma}$ dependence of $\bar{\varphi}$ for fixed N_{ag} exhibits a nonmonotonic behavior. Here, we explain this nonmonotonic dependence focusing on the results for $N_{ag} \geq 300$. For $\dot{\gamma} \leq 0.005$, $\bar{\varphi}$ decreases as $\dot{\gamma}$ increases, indicating that micelles align more in the flow direction for larger $\dot{\gamma}$. In contrast, for $\dot{\gamma} > 0.005$, $\bar{\varphi}$ decreases more slowly and slightly increases for $\dot{\gamma} \geq 0.02$. This is an intriguing phenomenon because $\bar{\varphi}$ of polymers monotonically decreases as $\dot{\gamma}$ increases, as described below (see Fig. 8). Interestingly, the saturation of alignment was also reported for amphiphilic Janus colloids,[47] which suggests the general alignment behavior of self-assembled clusters. In the next subsection, we will explore the origin of the alignment behavior by evaluating the micellar lifetime under shear flow.

Before closing this subsection, we refer to the results without using conditional statistics. We define $\bar{\Phi}$ as $\bar{\varphi}$ obtained with eqn (14) using all the data for micelles with $N_{ag} \geq 50$. In Fig. 4, we show $\bar{\Phi}$ as a function of $\dot{\gamma}$. In the case of the examined parameters, since a sufficient number of micelles with $N_{ag} \gtrsim N_\Lambda$ exist in the system, $\bar{\varphi}$ for $N_{ag} \gtrsim N_\Lambda$ and $\bar{\Phi}$ exhibit similar behavior. Specifically, $\bar{\Phi}$ does not decrease toward zero when increasing $\dot{\gamma}$, which was also observed in a previous study[31] modeling linear micelles as breakable bead-spring chains. However, due to the contributions from micelles with $N_{ag} \lesssim N_\Lambda$, $\bar{\Phi}$ is larger than $\bar{\varphi}$ for $N_{ag} \gtrsim N_\Lambda$. In summary, since $\bar{\Phi}$ depends on $P(N_{ag})$, interpretation of $\bar{\Phi}$ may not be
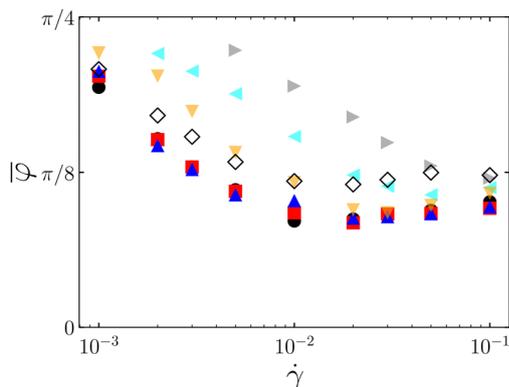
straightforward, especially when comparing results between different parameters.

3.2 Effect of scission

In the previous subsection, we have seen that $\bar{\varphi}$ of wormlike micelles exhibits a nontrivial dependence on $\dot{\gamma}$. To reveal its origin, we investigate the effect of scission on micellar alignment. To quantitatively evaluate micellar scission, we focus on the micellar lifetime t_b defined as the time between micellar birth and scission. We estimate a survival function $S(t_b)$, which gives the probability that micelles survive beyond a certain time t_b, using the Kaplan–Meier method.[48] Then, we fit $S(t_b)$ with $C_0 \exp(-t_b/\tau_b)$ to obtain the average lifetime τ_b. The definition of micellar scission and the method to evaluate τ_b are the same as in our previous study.[32] In this subsection, we will show the results of micelles with N_{ag} larger than N_Λ because more than 65% of surfactants in the system belong to micelles with $N_{ag} \gtrsim N_\Lambda$ at equilibrium. In addition, micelles with $N_{ag} \gtrsim N_\Lambda$ have the slowest timescale in the system as described in Section 4. In other words, they align most in the flow direction. We will discuss the alignment of micelles with $N_{ag} \lesssim N_\Lambda$ in Section 4.

To explore the relationship between alignment and scission, we show $\dot{\gamma}$ dependence of $\bar{\varphi}$ and τ_b for various N_{ag} ($> N_\Lambda$) in Fig. 5. To focus on the flow effect, we normalize τ_b by the value τ_b^0 at equilibrium for given N_{ag}. We find that τ_b/τ_b^0 also follows a single function of $\dot{\gamma}$ irrespective of N_{ag} ($> N_\Lambda$) as well as $\bar{\varphi}$. The bottom panel of Fig. 5 demonstrates that $\tau_b/\tau_b^0 \simeq 1$ for $\dot{\gamma} \lesssim 0.005$, indicating that flow-induced scission does not occur, whereas $\tau_b/\tau_b^0 \lesssim 1$ for $\dot{\gamma} \gtrsim 0.005$ due to flow-induced scission. We show this threshold shear rate $\dot{\gamma}_c$ (=0.005) for flow-induced scission in Fig. 5 to emphasize the effect of flow-induced scission. The top panel of Fig. 5 demonstrates that the alignment behavior changes around $\dot{\gamma}_c$. This indicates that
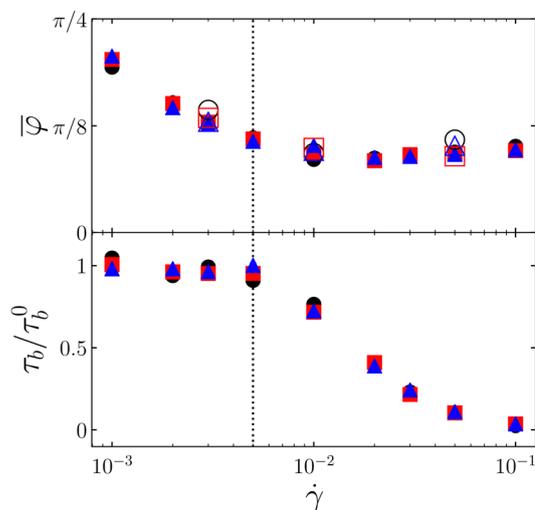

Fig. 4 Mean orientation angle $\bar{\varphi}$ of micelles as a function of the shear rate $\dot{\gamma}$ for $N_{ag} = 70$ (▶), 90 (◀), 130 (▼), 300 (●), 400 (■) and 500 (▲). For comparison, $\bar{\Phi}$ defined as $\bar{\varphi}$ obtained with all the data for micelles with $N_{ag} \geq 50$ is plotted (◇).

Fig. 5 Shear-rate $\dot{\gamma}$ dependence of the mean orientation angle $\bar{\varphi}$ (top panel) and the average lifetime τ_b (bottom panel) normalized by the value τ_b^0 at equilibrium for $N_{ag} = 300$ (●), 400 (■), and 500 (▲). The black dotted line indicates $\dot{\gamma} = \dot{\gamma}_c$. Open symbols in the top panel indicate the results of the larger system ($N = 3\,000\,000$).

flow-induced scission, which occurs for $\dot{\gamma} \gtrsim \dot{\gamma}_{\mathrm{c}}$, suppresses micellar alignment. It is worth emphasizing that Fig. 5 shows $\bar{\varphi}$ of micelles with a given N_{ag} obtained with conditional statistics instead of the average values over all the micelles. Thus, the increase in the number of small micelles due to flow-induced scission cannot explain the suppression of alignment. Although the present study focuses on the relationship between alignment and scission of micelles under shear flow, their effect on the rheological properties is an important aspect. In our previous study,[32] we have shown that the considered solutions have viscoelasticity and exhibit shear thinning. In this system, both alignment and flow-induced scission contribute to the shear thinning. Constitutive models based on the microscopic dynamics and kinetics of micelles (*e.g.* ref. 49) will allow a systematic study on the effect of alignment and flow-induced scission on the rheological properties, which is an important near-future study.

To confirm whether finite system sizes affect micellar alignment, we show the results of the system composed of $N = 3\,000\,000$ particles in Fig. 5. Since these results agree with those of $N = 648\,000$, finite system sizes have little effect on the micellar alignment. In the next section, we demonstrate that the nontrivial $\dot{\gamma}$ dependence of $\bar{\varphi}$ (Fig. 5) is specific to wormlike micelles by conducting a similar analysis for polymer models without scission.

Before closing this subsection, we refer to the orientational dynamics of micelles before scission. To observe the typical dynamics of micelles before scission, we show φ of micelles that survive for $O(\tau_{\mathrm{b}})$ as a function of time $t - t^*$ in Fig. 6. Here, $\dot{\gamma} = 0.01$, and t^* is the time when scission occurs. Since τ_{b} is smaller than the rotational relaxation time τ_{r} for $N_{\mathrm{ag}} = 300$ as described in Section 4.1, φ does not exhibit significant variations. This is evident by observing that φ of micelles with $N_{\mathrm{ag}} = 130$, for which $\tau_{\mathrm{b}} \gtrsim \tau_{\mathrm{r}}$, fluctuates between $-\pi/2$ and $\pi/2$ before scission. Consequently, micellar recombination plays an essential role in the distribution of φ when $\tau_{\mathrm{b}} \lesssim \tau_{\mathrm{r}}$. Thus it is an important near-future study to investigate micellar alignment in terms of recombination.[34,50,51]
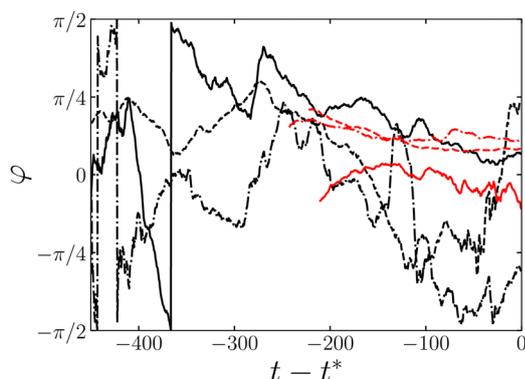

Fig. 6 Orientation angle φ of micelles that survive for $O(\tau_{\mathrm{b}})$ as a function of time $t - t^*$ before scission for $\dot{\gamma} = 0.01$. Different colors correspond to different values of N_{ag}: black, 130; red, 300. Different line styles correspond to different samples of micelles.

4. Discussion

4.1 Comparison with polymers

Comparing the mean orientation angle $\bar{\varphi}$ with the average lifetime τ_{b} has demonstrated that flow-induced scission suppresses micellar alignment (Fig. 5). Here, we compare the alignment of micelles with that of polymers to demonstrate the unique properties of micellar alignment.

Since wormlike micelles and polymers have different time-scales, we introduce the Weissenberg number $\mathrm{Wi} = \tau\dot{\gamma}$ defined as the product of the longest relaxation time τ and the shear rate $\dot{\gamma}$. We estimate τ of polymers by fitting the autocorrelation function $C(t)$ of the end-to-end vector with an exponential function $C_0 \exp(-t/\tau)$.[40] We obtain $\tau = 148$ in the case of the examined parameters.

We evaluate the longest relaxation time $\tau(N_{\mathrm{ag}})$ of unentangled micelles from the rotational relaxation time $\tau_{\mathrm{r}}(N_{\mathrm{ag}})$ and the average lifetime $\tau_{\mathrm{b}}(N_{\mathrm{ag}})$. Specifically, we use the formula

$$\tau(N_{\mathrm{ag}}) = \begin{cases} \tau_{\mathrm{r}}(N_{\mathrm{ag}}) & (N_{\mathrm{ag}} < N_\Lambda) \\ \tau_\Lambda & (N_{\mathrm{ag}} \geq N_\Lambda) \end{cases} \quad (16)$$

proposed in our previous study.[32] Here, we introduce a certain aggregation number N_Λ which satisfies $\tau_{\mathrm{r}}(N_\Lambda) = \tau_{\mathrm{b}}(N_\Lambda)$ and define τ_Λ as $\tau_{\mathrm{r}}(N_\Lambda)$. Fig. 7 shows the schematic of the longest relaxation time. In general, τ_{r} is a monotonically increasing function of N_{ag}.[32] However, relaxation modes such that $\tau_{\mathrm{r}}(N_{\mathrm{ag}}) > \tau_{\mathrm{b}}(N_{\mathrm{ag}})$ disappear due to the scission of micelles. Therefore, the intersection of $\tau_{\mathrm{r}}(N_{\mathrm{ag}})$ and $\tau_{\mathrm{b}}(N_{\mathrm{ag}})$ determines the largest timescale in the system. In other words, N_Λ defines
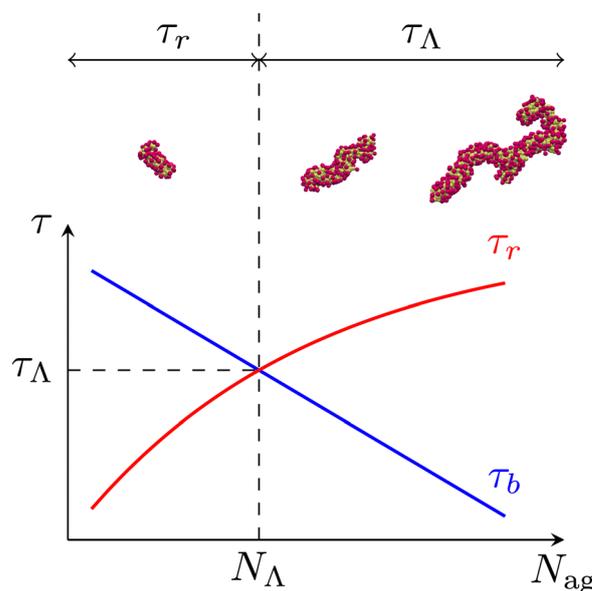

Fig. 7 Schematic of the longest relaxation time of micelles. The intersection of the rotational relaxation time τ_{r} and the average lifetime τ_{b} defines τ_Λ and N_Λ. Since τ_{b} is larger than τ_{r} for $N_{\mathrm{ag}} \lesssim N_\Lambda$, the rotational relaxation of micelles is not affected by their scission. In contrast, relaxation modes such that $\tau_{\mathrm{r}} \gtrsim \tau_\Lambda$ disappear due to the rapid scission of large micelles with $N_{\mathrm{ag}} \gtrsim N_\Lambda$. As a result, micelles with $N_{\mathrm{ag}} \gtrsim N_\Lambda$ are characterized by a common longest relaxation time τ_Λ.

the largest segment that behaves similarly to polymer chains (*i.e.*, chains without scission kinetics). Consequently, micelles with $N_{ag} \gtrsim N_\Lambda$ have a common longest relaxation time τ_Λ. This is consistent with the fact that $\bar{\varphi}$ and τ_b/τ_b^0 are independent of N_{ag} ($>N_\Lambda$) for fixed $\dot{\gamma}$ (Fig. 5). The methods to evaluate τ_r and τ_b are the same as in our previous study.[32] We obtain $\tau(70) = 72$, $\tau(90) = 203$, $\tau(130) = 586$, $\tau(300) = \tau(400) = \tau(500) = \tau_\Lambda = 796$ and $N_\Lambda = 169$.

Fig. 8 shows Wi dependence of $\bar{\varphi}$ for polymers and micelles. We confirm that $\bar{\varphi}$ of polymers obeys $\bar{\varphi} \propto \mathrm{Wi}^{-0.45}$ for Wi $\gtrsim 1$. A similar power law was reported in previous studies,[16,46,52,53] with a slightly different definition of a mean orientation angle. It is interesting to focus on the threshold Weissenberg number $\mathrm{Wi}_c = \tau_\Lambda \dot{\gamma}_c$ for flow-induced scission of micelles with $N_{ag} \gtrsim N_\Lambda$. The alignment behavior of micelles with $N_{ag} \gtrsim N_\Lambda$ deviates from that of polymers above Wi_c. Two important features are evident in this result. First, we confirm that $\bar{\varphi}$ of wormlike micelles and polymers collapse on a single function of Wi for Wi $\lesssim \mathrm{Wi}_c$, indicating the similar alignment behavior of worm-like micelles and polymers when flow-induced scission does not occur. In addition, this collapse verifies that eqn (16) proposed in our previous study[32] yields a quantitatively valid value of $\tau(N_{ag})$. Second, wormlike micelles have larger values of $\bar{\varphi}$ than polymers for Wi $\gtrsim \mathrm{Wi}_c$, indicating that flow-induced scission suppresses micellar alignment compared with polymers. So far, we have mainly focused on micelles with $N_{ag} \gtrsim N_\Lambda$. Here, we investigate the alignment of micelles with $N_{ag} \lesssim N_\Lambda$ in a similar way. Fig. 8 demonstrates that $\bar{\varphi}$ of micelles with $N_{ag} \lesssim N_\Lambda$ collapse on the same function for Wi $\lesssim \mathrm{Wi}_c$. This collapse shows that we can consider N_{ag} dependence of $\bar{\varphi}$ shown in Fig. 4 by using eqn (16). Similarly to micelles with $N_{ag} \gtrsim N_\Lambda$, $\bar{\varphi}$ of micelles with $N_{ag} \lesssim N_\Lambda$ is larger than that of polymers for Wi $\gtrsim \mathrm{Wi}_c$. Thus, the alignment of micelles with $N_{ag} \lesssim N_\Lambda$ is also suppressed for high shear rates. However, since $\bar{\varphi}$ has different values depending on N_{ag} for fixed Wi ($\gtrsim \mathrm{Wi}_c$), more detailed investigations are required to explain the degree of the alignment suppression. In the following, we again focus on the alignment of wormlike micelles with
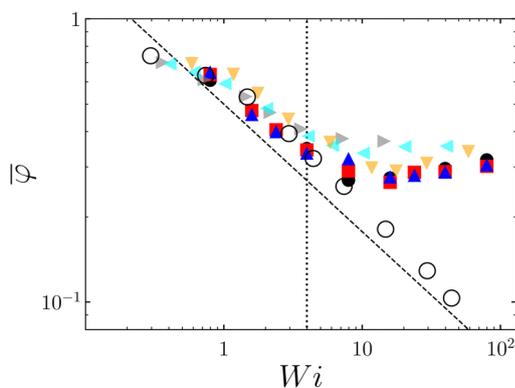
$N_{ag} \gtrsim N_\Lambda$, which are characterized by a common longest relaxation time τ_Λ.

We also confirm the suppression of micellar alignment through visualization of wormlike micelles and polymers for given Wi. For surfactant solutions, we define the Weissenberg number of the system as Wi = $\tau_\Lambda \dot{\gamma}$. We first focus on the alignment of wormlike micelles and polymers for Wi $\lesssim \mathrm{Wi}_c$, where flow-induced scission of micelles does not occur. Fig. 9(a) shows micelles with $200 \leq N_{ag} \leq 600$ for Wi = 2.4, and Fig. 9(c) shows some polymers which are randomly chosen for Wi = 3.0. They exhibit a qualitatively similar alignment behavior for Wi $\lesssim \mathrm{Wi}_c$. Incidentally, since surfactants consist of three DPD particles, micelles are slightly thicker than polymers. Indeed, the mean end-to-end distance of surfactants gives a rough estimate of the micellar radius $R \simeq 1.43$. Using longer surfactant models will reveal the effect of micellar thickness on alignment.

Next, we investigate their alignment for Wi $\gtrsim \mathrm{Wi}_c$, where flow-induced scission occurs. Fig. 9(b) shows micelles with $200 \leq N_{ag} \leq 600$ for Wi = 48, and Fig. 9(d) shows some polymers which are randomly chosen for Wi = 44. Note that, for clarity, we use the data for $\phi = 0.1$ in Fig. 9(b) because the number of micelles with $200 \leq N_{ag} \leq 600$ significantly decreases for large Wi due to flow-induced scission. We have confirmed that wormlike micelles exhibit similar alignment properties for $\phi = 0.1$ as in the case of $\phi = 0.05$. We observe in Fig. 9(d) that polymers considerably align in the flow direction, whereas wormlike micelles slightly tilt from the flow direction in Fig. 9(b). These observations are consistent with the quantitative results shown in Fig. 8. We then conclude that visualization also demonstrates the suppression of micellar alignment for Wi $\gtrsim \mathrm{Wi}_c$. In the next subsection, we consider the mechanism of
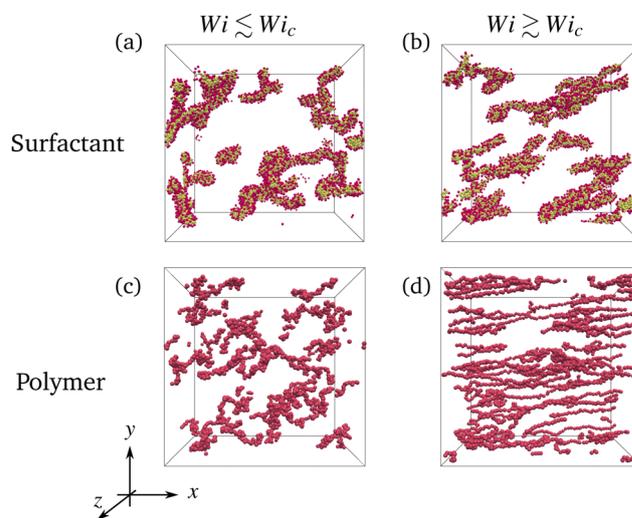
Fig. 9 Visualization of micelles with $200 \leq N_{ag} \leq 600$ for (a) Wi = 2.4 and (b) Wi = 48, and polymers for (c) Wi = 3.0 and (d) Wi = 44. Hydrophilic and hydrophobic particles are indicated in red and yellow, respectively (a and b). The number N_m of beads in a polymer is 50, and some of the polymers in the system are shown for clarity (c and d). The volume fraction ϕ of surfactants and polymers is (a, c and d) 0.05 and (b) 0.1.
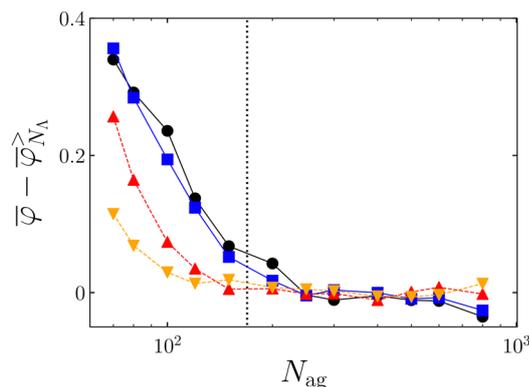
Fig. 8 Mean orientation angle $\bar{\varphi}$ as a function of the Weissenberg number Wi for polymers (○) and micelles: $N_{ag} = 70$ (▶), 90 (◀), 130 (▼), 300 (●), 400 (■) and 500 (▲). The vertical black dotted line indicates Wi = Wi_c. The black dashed line indicates $\bar{\varphi} \propto \mathrm{Wi}^{-0.45}$.

Fig. 10 Difference between the mean orientation angle $\bar{\varphi}$ and its average $\bar{\varphi}^{>}_{N_\Lambda}$ over micelles with $N_{ag} \geq N_\Lambda$ as a function of N_{ag}. Different symbols denote the results for different values of the shear rate: $\dot{\gamma}$ = 0.003, ●; 0.005, ■; 0.02, ▲; 0.05, ▼. Solid lines indicate the results for $\dot{\gamma} \leq \dot{\gamma}_c$ and dashed lines indicate those for $\dot{\gamma} > \dot{\gamma}_c$. The vertical black dotted line indicates N_Λ at equilibrium.

the suppression of micellar alignment focusing on the effective longest relaxation time under shear flow.

4.2 Effective longest relaxation time

We have shown that, for high shear rates, flow-induced scission occurs (Fig. 5) and suppresses micellar alignment compared with polymers (Fig. 8 and 9). This subsection demonstrates that flow-induced scission suppresses micellar alignment for fixed N_{ag} by reducing the effective longest relaxation time. As mentioned above, we focus on micelles with $N_{ag} \gtrsim N_\Lambda$. Such micelles have a common longest relaxation time τ_Λ and exhibit the most significant alignment of all the micelles in the system.

Let us now demonstrate that the decrease in the effective longest relaxation time τ_Λ causes the suppression of micellar alignment for high shear rates. Here, we propose a scenario that flow-induced scission reduces τ_b for $\dot{\gamma} \gtrsim \dot{\gamma}_c$ and then shifts τ_Λ and N_Λ shown in Fig. 7 towards lower values. To verify this scenario, we focus on the fact that micelles with $N_{ag} \gtrsim N_\Lambda$ are characterized by a common longest relaxation time τ_Λ. On the basis of this fact, we investigate whether N_Λ changes for $\dot{\gamma} \gtrsim \dot{\gamma}_c$ to confirm the reduction of τ_Λ. Fig. 10 shows $\bar{\varphi}$ as a function of N_{ag} for various $\dot{\gamma}$. Note that, for clarity, we subtract the average value $\bar{\varphi}^{>}_{N_\Lambda}$ over micelles with $N_{ag} \geq N_\Lambda$ from $\bar{\varphi}$ for each $\dot{\gamma}$. In Fig. 10, we show N_Λ at equilibrium by a vertical dotted line for comparison. For $\dot{\gamma} \leq \dot{\gamma}_c$, the behavior of $\bar{\varphi}$ changes around N_Λ. For $N_{ag} \lesssim N_\Lambda$, $\bar{\varphi}$ depends on N_{ag} because the micellar alignment is characterized by $\tau_r(N_{ag})$. In contrast, since τ_Λ is a common longest relaxation time of micelles with $N_{ag} \gtrsim N_\Lambda$, $\bar{\varphi}$ is independent of N_{ag} for $N_{ag} \gtrsim N_\Lambda$. Most notably, for $\dot{\gamma} > \dot{\gamma}_c$, the plateau regime of $\bar{\varphi}$ extends to a lower N_{ag} as $\dot{\gamma}$ increases. This indicates that N_Λ decreases as $\dot{\gamma}$ increases. In other words, the effective longest relaxation time also decreases for $\dot{\gamma} > \dot{\gamma}_c$. We, therefore, conclude that flow-induced scission promotes micellar scission and reduces the effective longest relaxation time τ_Λ, leading to the suppression of micellar alignment even for fixed N_{ag}.

5. Conclusions

We have conducted DPD simulations of nonionic surfactant solutions under shear flow to investigate the effect of scission on the alignment of wormlike micelles. The most important conclusion is that flow-induced scission suppresses micellar alignment even for fixed aggregation numbers N_{ag}. One may think that the suppression is obvious because flow-induced scission shortens micelles, *i.e.*, decreases N_{ag}, thus promoting their rotational relaxation. However, we emphasize that the suppression of micellar alignment can occur even for fixed N_{ag}. We have verified the conclusion by evaluating the shear-rate $\dot{\gamma}$ dependence of the average lifetime τ_b and the mean orientation angle $\bar{\varphi}$ for fixed N_{ag} (Fig. 5). Specifically, when $\dot{\gamma}$ exceeds a threshold shear rate $\dot{\gamma}_c$, τ_b becomes smaller than the value τ_b^0 at equilibrium and $\bar{\varphi}$ does not show such a decrease as when $\dot{\gamma} \lesssim \dot{\gamma}_c$. Comparing the alignment of micelles with that of polymers (*i.e.*, chains without scission kinetics) has provided further evidence that flow-induced scission suppresses micellar alignment for fixed N_{ag} (Fig. 8). To introduce the Weissenberg number Wi = $\tau\dot{\gamma}$ defined as the product of the longest relaxation time τ and $\dot{\gamma}$, we have evaluated τ of micelles using the method proposed in our previous study.[32] This method, which considers the effect of scission kinetics on micellar relaxation, has allowed us to compare the alignment of micelles and polymers appropriately. When Wi is smaller than the threshold Weissenberg number Wi$_c$ = $\tau\dot{\gamma}_c$ for flow-induced scission, $\bar{\varphi}$ of both micelles and polymers follows a single function of Wi. This collapse indicates the similar alignment behavior of micelles and polymers when flow-induced scission does not occur. In contrast, $\bar{\varphi}$ of micelles is larger than that of polymers for Wi $\gtrsim$ Wi$_c$. Such deviation of $\bar{\varphi}$ above Wi$_c$ confirms that flow-induced scission suppresses micellar alignment for fixed N_{ag}. Visualization also has shown that wormlike micelles tilt more from the flow direction than polymers for given Wi ($\gtrsim$Wi$_c$) (Fig. 9).

To explain the mechanism of the alignment suppression due to flow-induced scission, we have considered the effective longest relaxation time of micelles. Then we have demonstrated that the decrease in the effective longest relaxation time due to flow-induced scission plays a crucial role in suppressing micellar alignment. The concept of the micellar longest relaxation time (Fig. 7) predicts that the reduction of τ_b due to flow-induced scission decreases the effective longest relaxation time τ_Λ under shear flow. We have verified this prediction by evaluating N_{ag} dependence of $\bar{\varphi}$ (Fig. 10). According to the concept, when N_{ag} is larger than a certain aggregation number N_Λ, micelles are characterized by a common longest relaxation time τ_Λ. Indeed, we have found that when $\dot{\gamma}$ is smaller than $\dot{\gamma}_c$, $\bar{\varphi}$ is independent of N_{ag} for $N_{ag} \gtrsim N_\Lambda$. In contrast, for $\dot{\gamma} \gtrsim \dot{\gamma}_c$, the plateau regime of $\bar{\varphi}$ extends to a lower N_{ag} as $\dot{\gamma}$ increases. This observation shows that flow-induced scission reduces N_Λ and consequently reduces the effective Weissenberg number Wi = $\tau_\Lambda\dot{\gamma}$ of wormlike micelles with fixed N_{ag} ($\gtrsim N_\Lambda$) compared with the case without flow-induced scission, which is a major origin of the alignment suppression.

In the present study, we have quantitatively shown that flow-induced scission suppresses micellar alignment even for fixed N_{ag} and qualitatively explained the mechanism of this phenomenon through the decrease in the effective longest relaxation time under shear flow. However, we have yet to quantitatively explain the alignment behavior of micelles for Wi $\gtrsim$ Wi$_c$, where flow-induced scission occurs. For example, it is not completely clear why $\bar{\varphi}$ exhibits the nonmonotonic dependence on Wi (Fig. 8). To explain the degree of alignment suppression, we first need to quantify the effective longest relaxation time. In addition, it is likely that we need to consider the direct coupling between the orientational dynamics and scission kinetics of individual micelles under shear flow. These are left for future studies.

Author contributions

Yusuke Koide: conceptualization, data curation, formal analysis, investigation, methodology, validation, visualization, writing – original draft, writing – review & editing. Susumu Goto: conceptualization, funding acquisition, project administration, resources, supervision, writing – original draft, writing – review & editing.

Conflicts of interest

There are no conflicts to declare.

Acknowledgements

Notes and references

1 C. M. White and M. G. Mungal, *Annu. Rev. Fluid Mech.*, 2008, **40**, 235–256.
2 J. L. Zakin, B. Lu and H.-W. Bewersdorff, *Rev. Chem. Eng.*, 1998, **14**, 253–320.
3 L. Warwaruk and S. Ghaemi, *J. Fluid Mech.*, 2021, **917**, A7.
4 S. A. Vanapalli, S. L. Ceccio and M. J. Solomon, *Proc. Natl. Acad. Sci. U. S. A.*, 2006, **103**, 16660–16665.
5 J. M. J. Den Toonder, A. A. Draad, G. D. C. Kuiken and F. T. M. Nieuwstadt, *Appl. Sci. Res.*, 1995, **55**, 63–82.
6 A. S. Pereira, R. M. Andrade and E. J. Soares, *J. Non-Newtonian Fluid Mech.*, 2013, **202**, 72–87.
7 E. J. Soares, *J. Non-Newtonian Fluid Mech.*, 2020, **276**, 104225.
8 Z. Chu, C. A. Dreiss and Y. Feng, *Chem. Soc. Rev.*, 2013, **42**, 7174.
9 S. Tamano, H. Ikarashi, Y. Morinishi and K. Taga, *J. Non-Newtonian Fluid Mech.*, 2015, **215**, 1–7.
10 B. Yu, F. Li and Y. Kawaguchi, *Int. J. Heat Fluid Flow*, 2004, **25**, 961–974.
11 A. Krope and L. C. Lipus, *Appl. Therm. Eng.*, 2010, **30**, 833–838.
12 C. A. Dreiss, *Soft Matter*, 2007, **3**, 956–970.
13 L. Zhong, M. Oostrom, M. J. Truex, V. R. Vermeul and J. E. Szecsody, *J. Hazard. Mater.*, 2013, **244–245**, 160–170.
14 P. A. Cornwell, *Int. J. Cosmet. Sci.*, 2018, **40**, 16–30.
15 C. M. Schroeder, R. E. Teixeira, E. S. Shaqfeh and S. Chu, *Phys. Rev. Lett.*, 2005, **95**, 018301.
16 C. M. Schroeder, R. E. Teixeira, E. S. G. Shaqfeh and S. Chu, *Macromolecules*, 2005, **38**, 1967–1978.
17 C.-C. Huang, R. G. Winkler, G. Sutmann and G. Gompper, *Macromolecules*, 2010, **43**, 10107–10116.
18 R. G. Winkler, *J. Chem. Phys.*, 2010, **133**, 164905.
19 J. B. Hayter and J. Penfold, *J. Phys. Chem.*, 1984, **88**, 4589–4593.
20 V. Croce, T. Cosgrove, C. A. Dreiss, S. King, G. Maitland and T. Hughes, *Langmuir*, 2005, **21**, 6762–6768.
21 S. Förster, M. Konrad and P. Lindner, *Phys. Rev. Lett.*, 2005, **94**, 017803.
22 M. Takeda, T. Kusano, T. Matsunaga, H. Endo, M. Shibayama and T. Shikata, *Langmuir*, 2011, **27**, 1731–1738.
23 C. R. López-Barrón, A. K. Gurnon, A. P. R. Eberle, L. Porcar and N. J. Wagner, *Phys. Rev. E*, 2014, **89**, 042301.
24 A. K. Gurnon, C. López-Barrón, M. J. Wasbrough, L. Porcar and N. J. Wagner, *ACS Macro Lett.*, 2014, **3**, 276–280.
25 B. Arenas-Gómez, C. Garza, Y. Liu and R. Castillo, *J. Colloid Interface Sci.*, 2020, **560**, 618–625.
26 J. P. King, C. S. G. Butler, S. W. Prescott, A. V. Sokolova, L. de Campo, A. P. Williams and R. F. Tabor, *Phys. Fluids*, 2022, **34**, 083104.
27 C.-C. Huang, H. Xu and J.-P. Ryckaert, *Europhys. Lett.*, 2008, **81**, 58002.
28 C.-C. Huang, J.-P. Ryckaert and H. Xu, *Phys. Rev. E*, 2009, **79**, 041501.
29 J. Wei, Y. Kawaguchi, B. Yu, F. Li and C. Zhang, *Nonlinear Dyn.*, 2010, **61**, 503–515.
30 A. Sambasivam, A. V. Sangwai and R. Sureshkumar, *Phys. Rev. Lett.*, 2015, **114**, 158302.
31 W. Carl, R. Makhloufi and M. Kröger, *J. Phys. II*, 1997, **7**, 931–946.
32 Y. Koide and S. Goto, *J. Chem. Phys.*, 2022, **157**, 084903.
33 M. Kröger and R. Makhloufi, *Phys. Rev. E*, 1996, **53**, 2531.
34 C.-C. Huang, H. Xu and J.-P. Ryckaert, *J. Chem. Phys.*, 2006, **125**, 094901.
35 J. T. Padding, W. J. Briels, M. R. Stukan and E. S. Boek, *Soft Matter*, 2009, **5**, 4367–4375.
36 J. T. Padding, E. S. Boek and W. J. Briels, *J. Chem. Phys.*, 2008, **129**, 074903.
37 P. Español and P. Warren, *Europhys. Lett.*, 1995, **30**, 191.
38 R. D. Groot and P. B. Warren, *J. Chem. Phys.*, 1997, **107**, 4423–4435.
39 K. Kremer and G. S. Grest, *J. Chem. Phys.*, 1990, **92**, 5057–5086.
40 W. Jiang, J. Huang, Y. Wang and M. Laradji, *J. Chem. Phys.*, 2007, **126**, 044901.

41 A. W. Lees and S. F. Edwards, *J. Phys. C: Solid State Phys.*, 1972, **5**, 1921.

42 D. J. Evans and G. Morriss, *Statistical Mechanics of Nonequilibrium Liquids*, Cambridge University Press, 2008.

43 A. Vishnyakov, M.-T. Lee and A. V. Neimark, *J. Phys. Chem. Lett.*, 2013, **4**, 797–802.

44 M.-T. Lee, R. Mao, A. Vishnyakov and A. V. Neimark, *J. Phys. Chem. B*, 2016, **120**, 4980–4991.

45 N. I. Fisher, *Statistical Analysis of Circular Data*, Cambridge University Press, 1995.

46 C. Aust, M. Kröger and S. Hess, *Macromolecules*, 1999, **32**, 5660–5672.

47 Y. Kobayashi, N. Arai and A. Nikoubashman, *Soft Matter*, 2020, **16**, 476–486.

48 E. L. Kaplan and P. Meier, *J. Am. Stat. Assoc.*, 1958, **53**, 457–481.

49 R. J. Hommel and M. D. Graham, *J. Non-Newtonian Fluid Mech.*, 2021, **295**, 104606.

50 B. O'Shaughnessy and J. Yu, *Phys. Rev. Lett.*, 1995, **74**, 4329–4332.

51 J. T. Padding and E. S. Boek, *Europhys. Lett.*, 2004, **66**, 756.

52 R. E. Teixeira, H. P. Babcock, E. S. G. Shaqfeh and S. Chu, *Macromolecules*, 2005, **38**, 581–592.

53 M. Q. Tu, M. Lee, R. M. Robertson-Anderson and C. M. Schroeder, *Macromolecules*, 2020, **53**, 9406–9419.